Received: 3 June 2019 | Revised: 17 September 2019 | Accepted: 15 December 2019

DOI: 10.1002/wics.1495

OVERVIEW

WIREs COMPUTATIONAL STATISTICS WILEY

Analysis of shape data: From landmarks to elastic curves

Karthik Bharath[1] | **Sebastian Kurtek**[2]

[1]School of Mathematical Sciences, University of Nottingham, Nottingham, UK

[2]Department of Statistics, The Ohio State University, Columbus, Ohio

Correspondence
Sebastian Kurtek, Department of Statistics, The Ohio State University, Columbus, OH.
Email: kurtek.1@stat.osu.edu

Funding information
Division of Computing and Communication Foundations, Grant/Award Numbers: 1740761, 1839252; Division of Mathematical Sciences, Grant/Award Numbers: 1613054, 1743943; National Cancer Institute, Grant/Award Number: R37 CA214955

Abstract

Proliferation of high-resolution imaging data in recent years has led to substantial improvements in the two popular approaches for analyzing shapes of data objects based on landmarks and/or continuous curves. We provide an expository account of elastic shape analysis of parametric planar curves representing shapes of two-dimensional (2D) objects by discussing its differences, and its commonalities, to the landmark-based approach. Particular attention is accorded to the role of reparameterization of a curve, which in addition to rotation, scaling and translation, represents an important shape-preserving transformation of a curve. The transition to the curve-based approach moves the mathematical setting of shape analysis from finite-dimensional non-Euclidean spaces to infinite-dimensional ones. We discuss some of the challenges associated with the infinite-dimensionality of the shape space, and illustrate the use of geometry-based methods in the computation of intrinsic statistical summaries and in the definition of statistical models on a 2D imaging dataset consisting of mouse vertebrae. We conclude with an overview of the current state-of-the-art in the field.

This article is categorized under:

Image and Spatial Data < Data: Types and Structure
Computational Mathematics < Applications of Computational Statistics

KEYWORDS

elastic curves, landmarks, non-Euclidean space, shape statistics

1 | INTRODUCTION

Shape is a fundamental property of objects. Statistical analysis of data pertaining to shape is predicated on our ability to mathematically represent shape, and to measure and quantify shape differences. The natural habitat, however, for mathematical representations of interesting shape data are non-Euclidean spaces. This demands an adaptation of standard statistical methods on linear spaces, or development of new ones based on explicit geometric considerations of the shape space.

As an example, consider the problem of characterization of objects present in two-dimensional (2D) images. The first step is to identify and extract the different aspects of the object within the image. One can consider pixel values on or around the object of interest, also commonly referred to as texture, or alternatively consider the boundary of the object of interest. This article is concerned only with the latter, although the former has been, and is, an active field of research (Humeau-Heurtier, 2019; Materka, 2004).

Depending on the resolution, the boundary of the object can be represented in (at least) two ways: a set of distinct 2D points on the object which represent certain special features of the object, or as a continuous curve on the plane. Then, the shape of the object under a certain representation can be intuitively understood as the geometric information of the object that is independent of variations due to translations, scaling and rotations. The point-set representation generally leads to *landmark-based methods*, whereas the representation using continuous curves naturally leads to *elastic shape analysis* methods. Both approaches lead to the understanding of a shape of an object as the associated equivalence class of objects that are related to the original object through a set of shape-preserving transformations.

Landmark-based methods in statistical shape analysis have been extensively studied over the years. The book *Statistical shape analysis*: *With applications in R* by Dryden and Mardia (2016) provides an excellent introduction and overview of the state-of-the-art on this topic. Curve representations of shape data, while studied by the mathematical and computer vision communities for several years (Joshi, Klassen, Srivastava, & Jermyn, 2007; Klassen & Srivastava, 2006; Klassen, Srivastava, Mio, & Joshi, 2004; Younes, 1998; Younes, Michor, Shah, Mumford, & Lincei, 2008; Zahn & Roskies, 1972), have only recently gained traction within the statistics community, mainly coinciding with the profusion of imaging data from biomedical applications. With this in mind, borrowing ideas and concepts liberally from the recently published book *Functional and shape data analysis* (Srivastava & Klassen, 2016), our aim in this overview article is to provide an expository account of analysis of 2D shape objects by describing the differences and commonalities between the two approaches (landmark-based and elastic curve-based), both from conceptual and operational perspectives.[1]

We adopt an informal style of exposition whereby the focus is on conveying the main ideas with minimal technicalities. We consider four key aspects of statistical shape analysis of data objects, presented in a natural order of progression: (a) mathematical representation, (b) choice of metric and shape distance, (c) statistical summaries under the chosen metric, and (d) statistical models. Geometrical considerations play a vital role in the exposition, in addition to the definition of the shape of an object as an equivalence class characterized by a class of transformations of the object that represent nuisance variation.

To concretize ideas, we consider a dataset of 2D images of the second thoracic (T2) mouse vertebrae, and demonstrate the features and utility of the curve-based approach on each of the four aspects. This dataset contains a total of 76 vertebrae divided into three groups: large (30 mice), small (23 mice), and control (30 mice). A detailed description of this dataset (section 1.4.1), along with a thorough statistical analysis under the landmark-based representation, are given in Dryden and Mardia (2016). More recently, this data was also analyzed under different representations in Cheng, Dryden, and Huang (2016), Strait, Kurtek, Bartha, and MacEachern (2017) and Cho, Asiaee, and Kurtek (2019). The entire dataset is available in R as part of the *shapes* package.[2]

1.1 | Related work

There has been a tremendous amount of shape analysis research in multiple disciplines including statistics, applied mathematics, computer science and different domain sciences, especially biology. The main differences between the methods usually boil down to the choice of representation and metric for shape comparison and statistical modeling. Here, we provide a brief look at some of the most prominent approaches to shape analysis in current literature.

The field of shape analysis can be traced back to the pioneering work of D'Arcy Thompson, a biologist/mathematician, and his book titled *On growth and form* (Thompson, 1917). In his approach, Thompson deformed objects of interest to make them appear more similar. Recently, deformation-based approaches have become extremely popular. The work in this area began with Grenander's deformable templates (Grenander & Miller, 1998; Joshi, Miller, & Grenander, 1997). This idea was later used to develop the general framework of large deformation diffeomorphic metric mapping (LDDMM) (Beg, Miller, Trouvé, & Younes, 2005), which can be used to study shapes of point sets (Glaunès, Vaillant, & Miller, 2004; Joshi & Miller, 2000), curves (Glaunès, Qiu, Miller, & Younes, 2008) and surfaces (Durrleman, Pennec, Trouvé, & Ayache, 2009; Vaillant & Glaunès, 2005). Recently, these methods have been extended to use varifolds as the shape representation (Charon & Truové, 2013). Deformable templates and LDDMM have proven to be extremely useful in computational anatomy for quantifying variability of anatomical shapes. Other popular 2D and three-dimensional (3D) shape representations include level sets (Malladi, Sethian, & Vemuri, 1996), medial axes (Bouix, Pruessner, Collins, & Siddiqi, 2001; Gorczowski et al., 2010; Siddiqi & Pizer, 2008), or point clouds (Almhdie, Léger, Deriche, & Lédée, 2007). Another recent approach to shape analysis has its roots in the field of topological data analysis wherein shapes of

objects are represented using a topological summary statistic called the smooth Euler characteristic transform (Crawford, Monod, Chen, Mukherjee, & Rabadán, 2019).

However, the two most widely utilized approaches in statistical shape analysis represent 2D objects via landmarks (Bookstein, 1992; Dryden & Mardia, 2016; Small, 1996) or curves (Klassen et al., 2004; Srivastava & Klassen, 2016; Srivastava, Klassen, Joshi, & Jermyn, 2011; Zahn & Roskies, 1972). Section 2.1 in Dryden and Mardia (2016) contains an interesting discussion on the historical context within which the field of statistical shape analysis based on landmark representations evolved, and contains many other relevant references. We also note that the elastic shape analysis framework for curves has been recently extended to the case of surfaces; see the recent book of Jermyn, Kurtek, Laga, and Srivastava (2017) for details.

1.2 | Applications of landmark- and curve-based shape analysis

Before proceeding with the mathematical and statistical description of the landmark- and curve-based frameworks for shape analysis, we briefly outline the many possible applications of these methods. One of the scientific areas where statistical shape analysis has played a prominent role is biology. Landmark-based methods especially have reached deep into various biological applications (Bookstein, 1984, 1996; Dryden & Mardia, 1993; Mardia & Dryden, 1989; O'Higgins & Dryden, 1992). More recently, curve-based methods have seen their own success in this setting; see Cho et al. (2019) for a detailed overview. Another promising area of applied research is in medical imaging. With recent advances in medical imaging acquisition technology, large datasets are becoming common. An important goal in medical imaging is to assess the morphology of anatomical structures for the purposes of disease detection or monitoring. While most research focuses on 3D shape analysis in this setting (Kurtek et al., 2011; Samir, Kurtek, Srivastava, & Canis, 2014), curve-based approaches have been used to model shapes of diffusion tensor magnetic resonance imaging fiber tracts (Kurtek, Srivastava, Klassen, & Ding, 2012), to assess variability in manual segmentation of medical images (Kurtek et al., 2013), and to model survival based on glioblastoma multiforme tumor shapes (Bharath, Kurtek, Rao, & Baladandayuthapani, 2018). Other popular applications of statistical shape analysis include biometrics (Kaziska & Srivastava, 2006; Samir, Srivastava, Daoudi, & Klassen, 2009; Srivastava, Samir, Joshi, & Daoudi, 2009), military (Joshi & Srivastava, 2009), activity recognition and modeling (Su, Kurtek, Klassen, & Srivastava, 2014), and anthropology (O'Higgins & Dryden, 1992), among others. We display a few applications of statistical shape analysis in Figure 1.

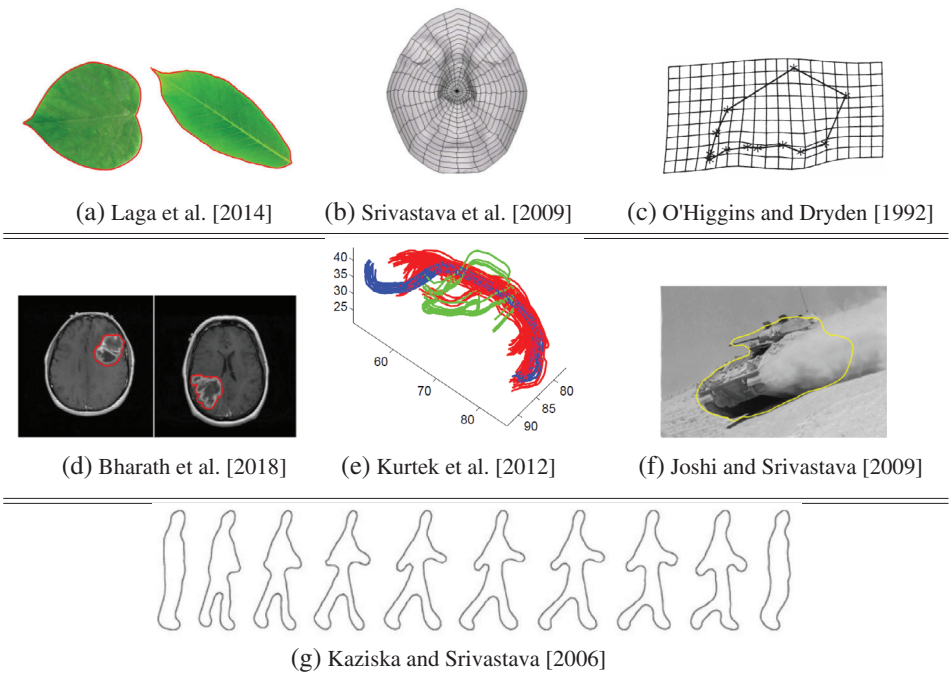

FIGURE 1 Applications of statistical shape analysis include (a) leaf shape classification, (b) facial recognition, (c) anthropology, (d) tumor shape modeling, (e) clustering of diffusion tensor magnetic resonance imaging fibers, (f) military defense, and (g) gait recognition

2 | MATHEMATICAL REPRESENTATION

Kendall (1984) states that the shape of an object is a geometric property that remains after scale, rotation and translation variabilities have been filtered out. This definition can be extended to the curve-based representation by requiring that variability due to reparametrization of the curve be removed as well, as it is shape-preserving. We first briefly review the shape representation for the landmark-based approach. Figure 2 shows four representations of a shape data object corresponding to a mouse vertebra. We will mainly be concerned with the landmark- and curve-based representations displayed in panels (b) and (c), respectively; we briefly comment on the curve-with-landmarks representation, shown in panel (d), in the final section of the article.

2.1 | Landmark-based approach

A set of N points in two dimensions on an object that establishes correspondence between objects are known as landmarks. They are typically classified as *scientific*, if they have been chosen by experts as being representative of a scientific property of the object (e.g., anatomical landmarks on organisms), *mathematical*, if they are points representing certain geometric or mathematical properties of the object (e.g., curvature, extrema), or *pseudo*, if they are just sampled along the boundary or outline of the object.

Landmarks in Cartesian coordinates on an object are arranged into a *configuration matrix* X of dimension $N \times 2$, and the corresponding set of configuration matrices associated with a sample of data objects is then referred to as the configuration space. Figure 2b shows six mathematical landmarks, labeled using different colors, extracted from the image in Figure 2a. The shape of a configuration matrix X is given by the set

$$[X] := \left\{ \sigma X O + \mathbf{1}_N x_0^T : \; O \in SO(2), \; x_0 \in \mathbb{R}^2, \; \sigma > 0 \right\},$$

where $SO(2)$ is the special orthogonal group $\{O \in \mathbb{R}^{2\times 2} : O^T O = O O^T = I_2, \det(O) = +1\}$ of rotation matrices and $\mathbf{1}_N$ is the vector of N ones. The shape of X, denoted as $[X]$, is the set of all possible similarity transformations of X, which rotate (using the matrix O), scale (using the positive scalar σ), and translate (using the two-vector x_0) X. Similarity transforms of X do not alter its shape, as understood using Kendall's definition. Note that the shape $[X]$ is an entire class of configurations that are related by similarity transforms.

The set of similarity transformations[3] $(\sigma, O, x_0) \in \mathbb{R}_+ \times SO(2) \times \mathbb{R}^2$ can be endowed with a group structure, which offers a nice algebraic characterization of the shape of X. Thus, $[X]$ is an equivalence class of configuration matrices of X, known as the *orbit* of X under the action of the above-mentioned group: a configuration matrix Y belongs to $[X]$ if it can be transformed to X using one or a combination of similarity transforms. The set of orbits $\{[X] : X \in \mathbb{R}^{N\times 2}\}$ forms the corresponding *quotient space*.

2.2 | Curve-based approach

In some applications, for example, the tumor shapes in Figure 1d, it may be costly or difficult to choose suitable landmarks for shape analysis. Instead of assigning mathematical or pseudo landmarks along the boundary of the object, a natural alternative would be to consider the entire outline while choosing a representation. While discretization

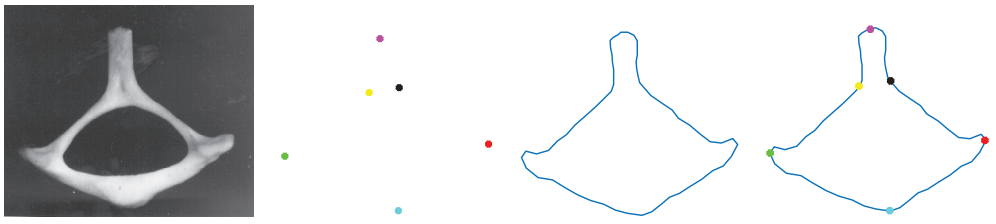

(a) (b) (c) (d)

FIGURE 2 Four different representations of a mouse vertebra: (a) grayscale image, (b) color-labeled landmarks, (c) curve, and (d) curve with color-labeled landmarks

becomes necessary at the implementation stage, the underlying data objects are continuous curves and should thus be modeled as such; as a result, in contrast to landmark-based approaches, discretization in curve-based shape analysis is only performed at the end. Furthermore, a curve-based shape representation allows one to properly define reparameterization invariance as seen in the following paragraph. Figure 2c shows the outline of the mouse vertebra extracted from the image in Figure 2a. Mathematically, the boundary of the mouse vertebra can be represented as a parameterized closed planar curve $\beta : \mathbb{S}^1 \to \mathbb{R}^2$, where $\mathbb{S}^1$ is the unit circle on the plane. The image of $t \mapsto \beta(t)$ captures the boundary of the object.

As with the landmark approach, the definition of the shape of β requires accounting for a set of nuisance transformations. In addition to similarity transformations, another important source of unwanted variability is the arbitrariness of the parameterization of β. That is, the domain $\mathbb{S}^1$ of the curve β is unobserved and not part of the data. Since any smooth one-to-one mapping of $\mathbb{S}^1$ to itself, preserving clockwise or anti-clockwise order, will not change the image of $t \mapsto \beta(t)$, the set of all such transformations also ascribe nuisance variability to the observed β. Another way of interpreting reparameterization variability is by relating the transformation to the speed of traversal along the domain $\mathbb{S}^1$, and noting that it has no bearing on the shape of the observed curve. This is illustrated in Figure 3. We start with a curve β, which is sampled according to arc-length (red points with uniform sampling). To reparameterize β, we use a special function γ displayed in the figure using angles corresponding to coordinates on the unit circle.[4] The composition of β and γ results in a new nonlinear sampling of points on the curve (red points). Evidently, the class of all transformations of $\mathbb{S}^1$ preserving the shape of β is a large function class. But, it can be equipped with a group structure, and modeled as the set of one-to-one, smooth functions with a smooth inverse, which do not alter the order of traversal along $\mathbb{S}^1$. Thus, we consider $\Gamma := \{\gamma : \mathbb{S}^1 \to \mathbb{S}^1 : \gamma \text{ is an orientation preserving diffeomorphism}\}$, as the group of transformations that represent reparametrizations of a closed planar curve β.

From the above discussion, we see that the shape of a closed curve $\beta : \mathbb{S}^1 \to \mathbb{R}^2$ is given by the equivalence class

$$[\beta] := \{\sigma O(\beta \circ \gamma) + x_0 : O \in SO(2),\ x_0 \in \mathbb{R}^2,\ \sigma > 0,\ \gamma \in \Gamma\}.$$

The group corresponding to the above set of transformations is $\{(O, x_0, \sigma, \gamma) \in SO(2) \times \mathbb{R}^2 \times \mathbb{R}_+ \times \Gamma\}$. The shape $[\beta]$, as with the landmark approach, is the orbit under the action of this group. Figure 4a displays four mouse vertebra curves that have different translations, rotations and scales, but the same shape. Figure 4b provides a pictorial description of

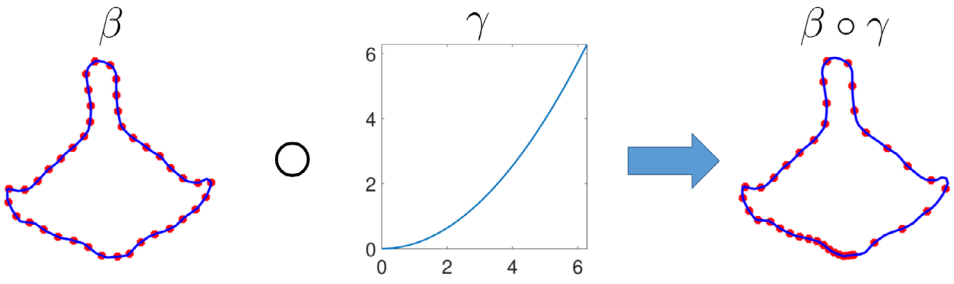

FIGURE 3 A mouse vertebra curve β reparameterized using a diffeomorphism of $\mathbb{S}^1$, γ (represented as an angle $[0, 2\pi)$), resulting in $\beta \circ \gamma$. The sampling of points according to the curve's parameterization is shown in red

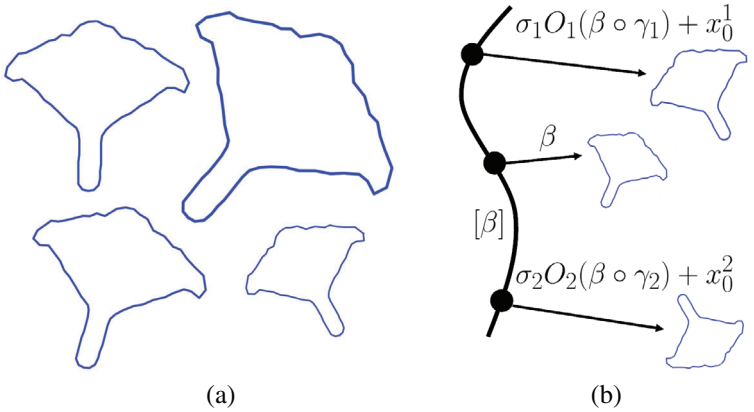

FIGURE 4 (a) Different similarity transformations applied to the same mouse vertebra. Note that all have the same exact shape. (b) Pictorial representation of an orbit of a curve

an orbit of a mouse vertebra. The three displayed curves correspond to three different points along the orbit and have the same exact shape.

Once a representation has been chosen, the shape of each object is a suitable equivalence class of transforms of the object. Data analysis works at the level of individual objects and not necessarily the equivalence classes. This issue will be dealt with next.

3 | GEOMETRY OF SHAPE SPACE AND METRIC

Geometric information about the shape of an object necessitates explicit considerations of the geometry of the space in which it resides, characterized by the important choice of a metric to measure shape differences. Broadly, the two most common approaches are *extrinsic* and *intrinsic*. The latter restricts attention wholly to the shape space, endows it with a Riemannian structure, and proceeds to compute quantities of interest using a Riemannian distance. The former embeds the shape space into a larger space, which is more amenable for calculation of desired quantities, and projects them back to the shape space. Our focus will be on intrinsic approaches to shape analysis. The main tool for statistical analysis is the metric, and the focus hence will mostly be on its choice; the corresponding geometry will only offer a convenient backdrop for the results.

3.1 | Landmark-based approach

Recall that the orbit $[X]$ is characterized by all possible scalings, translations and rotations of a configuration matrix X. The program is to remove scaling and translation variability of X by suitable transformations, such that the orbit $[X]$ then contains rotated versions of X only.[5]

In two dimensions, the geometry of the shape space can be nicely described with complex arithmetic by identifying $\mathbb{R}^2$ with the complex plane $\mathbb{C}$. Given a configuration $X \in \mathbb{R}^{N\times 2}$, we can identify a landmark x_j (row j of X) in $\mathbb{R}^2$ with a point on the complex plane $\mathbb{C}$ as $z_j = x_{j,1} + ix_{j,2}$ where $i = \sqrt{-1}$. A configuration X can then be mapped to a point $\mathbf{z} \in \mathbb{C}^N$ in the N-dimensional complex space.

Translation and scaling variability can be removed by translating the center of $\mathbf{z}$ to the origin, and rescaling $\mathbf{z}$ to have unit norm. This can be achieved by applying the transform $z_j \mapsto \left(z_j - N^{-1}\sum_{j=1}^{N} z_j\right)$ followed by $\mathbf{z} \mapsto \mathbf{z}/|\mathbf{z}|$, where $|\cdot|$ here is the standard Euclidean norm. The resulting set of $\mathbf{z}$ following the transforms is referred to as the *preshape space*, since rotational variability is yet to be removed. Formally, the preshape space is

$$\mathcal{C}^N := \left\{ \mathbf{z} \in \mathbb{C}^N : \frac{1}{N}\sum_{j=1}^{N} z_j = 0,\ |z| = 1 \right\},$$

which is the unit sphere in the N-dimensional complex space. We move from the preshape space to the shape space by re-defining the orbit of $\mathbf{z}$ only with respect to rotations. Indeed, each rotation in two dimensions can be parameterized by a single angle, and hence $SO(2) = \mathbb{S}^1$. Thus, we have that $[\mathbf{z}] = \left\{ e^{i\theta}\mathbf{z} : \theta \in \mathbb{S}^1 \right\}$. The set of orbits $\{[\mathbf{z}]\}$ is referred to as the *shape space*, denoted as $\mathcal{S}_2^N$. We see that $\mathcal{S}_2^N$ can be identified with the complex projective space $\mathbb{CP}^{N-1}$.

Thus, for landmarks in two dimensions, the shape space $\mathcal{S}_2^N$ can be endowed with a nice geometry upon choosing a Riemannian metric. One convenient way to define a distance on the shape space is to choose a metric on the preshape space that is invariant to rotations.[6] A natural candidate for a distance on $\mathcal{C}^N$ is the shortest great circle distance

$$\rho(\mathbf{z}_1, \mathbf{z}_2) := \arccos |\mathbf{z}_1^* \mathbf{z}_2|, \quad \mathbf{z}_1, \mathbf{z}_2 \in \mathcal{C}^N,$$

where $\mathbf{z}^*$ denotes the complex conjugate of $\mathbf{z}$, and $|\mathbf{z}| = \sqrt{\mathbf{z}^*\mathbf{z}}$ its modulus. On the preshape sphere $\mathcal{C}^N$, the distance ρ can be interpreted as the smallest angle between complex vectors $\mathbf{z}_1$ and $\mathbf{z}_2$. It is easy to see that ρ is invariant to simultaneous rotations $e^{i\theta}$ of $\mathbf{z}_1$ and $\mathbf{z}_2$ with respect to any $\theta \in \mathbb{S}^1$. Using the invariance of ρ to rotations, we can define the *Riemannian shape distance* between $[\mathbf{z}_1]$ and $[\mathbf{z}_2]$ as

$$\rho_s([\mathbf{z}_1],[\mathbf{z}_2]) := \min_{\theta\in\mathbb{S}^1} \rho\left(e^{i\theta}\mathbf{z}_1, \mathbf{z}_2\right) .$$

3.2 | Curve-based approach

While nuisance variability due to translation, scaling and rotation can be taken care of in a manner similar to the landmark case, reparameterization variability brings about a new set of challenges. Previous approaches removed this source of variability by normalizing parameterizations to arc-length (Klassen et al., 2004; Zahn & Roskies, 1972). However, this fixes the correspondence of points across curves and results in suboptimal matching of their geometric features. In contrast, the elastic shape analysis approach that is our focus in this article, allows for computation of "optimal" parameterizations, resulting in more natural deformations between and statistics of shapes. In the notation introduced earlier, a reparameterization of the curve β is given by composition with a smooth invertible $\gamma \in \Gamma$.

Recall that the orbit $[\beta]$ of β represents its shape. Before performing a stage-wise removal of nuisance variaiblity, and defining the preshape space, we note a major obstacle in following the program used for landmarks. Analogous to the standard Euclidean metric in the landmark setting, consider the standard $\mathbb{L}^2$ distance defined as $||\beta_1 - \beta_2||_2 = \left(\int_0^{2\pi} ||\beta_1|t| - \beta_2|t||^2 dt\right)^{1/2}$, where $|\cdot|$ denotes the Euclidean norm in $\mathbb{R}^2$. It is easy to see that

$$\|\beta_1 - \beta_2\|_2 \neq \|\beta_1 \circ \gamma - \beta_2 \circ \gamma\|_2$$

for general $\gamma \in \Gamma$, and hence this metric is not invariant to reparameterization.

How can we overcome this fundamental challenge? First, we introduce an alternative representation of a parameterized curve. Let the square-root velocity function (SRVF) of a curve β be given by $q = \frac{\dot{\beta}}{\sqrt{|\dot{\beta}|}}$, where again $|\cdot|$ is the Euclidean norm in $\mathbb{R}^2$ and $\dot{\beta}$ is the derivative of β. It is easy to see that this representation is translation invariant as its definition involves first derivatives only. Furthermore, if β is absolutely continuous then its SRVF is square-integrable, that is, an element of the space $\mathbb{L}^2\left(\mathbb{S}^1, \mathbb{R}^2\right)$[2012] (Robinson, 2012) (henceforth denoted by $\mathbb{L}^2$ for brevity). Finally, the inverse mapping from an SRVF q to the corresponding curve β is simply given by $\beta(t) = \beta(0) + \int_0^t q(s)\,|\,q(s)\,|\,ds$ for all t. In fact, the SRVF of β is unique up to translations, and vice versa. The natural metric on the SRVF space is then given by the $\mathbb{L}^2$ metric.

The above discussion begs the question: Why did we introduce the SRVF? It turns out that the $\mathbb{L}^2$ distance on the space of SRVFs is invariant to reparameterizations. First, one can easily check that the SRVF of a reparameterized curve $\beta \circ \gamma$ is given by $(q \circ \gamma)\sqrt{\dot{\gamma}}$. Then, one can check that for two SRVFs $q_1, q_2 \in \mathbb{L}^2$, and a reparameterization $\gamma \in \Gamma$, the following holds true: $\|q_1 - q_2\|_2 = \|(q_1 \circ \gamma)\sqrt{\dot{\gamma}} - (q_2 \circ \gamma)\sqrt{\dot{\gamma}}\|_2$, making the $\mathbb{L}^2$ metric invariant under reparameterizations. Another compelling reason for introducing the SRVF representation for shape analysis is that the $\mathbb{L}^2$[2011] metric on the space of SRVFs corresponds to a specific instance of an elastic metric on the original space of absolutely continuous curves (Srivastava et al., 2011). This elastic metric measures the amount of stretching and bending needed to deform one shape into another, providing a natural interpretation (Mio, Srivastava, & Joshi, 2007).

As mentioned earlier, the SRVF q is automatically translation invariant. To remove scaling, we consider curves of unit length only; an equivalent condition on SRVFs is that their $\mathbb{L}^2$ norm is equal to one. The set of all such SRVFs is the unit Hilbert sphere in $\mathbb{L}^2$ denoted by S_∞ (Lang, 2001); it is the preshape space denoted by

$$\mathcal{C} = \left\{q : \mathbb{S}^1 \to \mathbb{R}^2 : \ \|q\|_2^2 = 1\right\}.^7$$

This preshape space is analogous to the unit sphere $\mathcal{C}^N$ for the case of N landmarks in $m = 2$ dimensions. Rotation and reparameterization variabilities now need to be dealt with. Note that the SRVF of a rotated curve $O\beta$, where $O \in SO(2)$, is simply Oq. Thus, the orbit of q is

$$[q] = \left\{ O(q \circ \gamma)\sqrt{\dot{\gamma}} : O \in SO(2), \gamma \in \Gamma \right\};$$

this orbit contains all possible rotations and reparameterizations of the SRVF q and allows us to unify these different elements of the preshape space as a single data object, resulting in the shape space of interest $\mathcal{S} = \{[q] : q \in \mathcal{C}\}$.

As with the landmark shape space $\mathcal{S}_2^N$, we induce a distance on $\mathcal{S}$ through a Riemannian distance on the preshape space $\mathcal{C}$ invariant to simultaneous rotations and reparameterizations. Let

$$\rho(q_1, q_2) := \arccos(\langle\langle q_1, q_2 \rangle\rangle) := \arccos\left(\int_0^{2\pi} \langle q_1(t), q_2(t) \rangle dt \right)$$

be the distance between q_1 and q_2 on $\mathcal{C}$, where $\langle \cdot, \cdot \rangle$ is the standard inner product in $\mathbb{R}^2$. Accordingly, ρ represents the angle (length of shortest arc) between the two points on the unit sphere $S_\infty = \mathcal{C}$. This shortest arc is given by the parameterized curve

$$\alpha(\tau) = \frac{1}{\sin(\nu)}(\sin(\nu(1-\tau))q_1 + \sin(\nu\tau)q_2), \quad \tau \in [0,1], \tag{1}$$

where $\nu = \rho(q_1, q_2)$. Note that the distance ρ is invariant to rotations and reparameterizations, as discussed earlier. As a consequence, as with the landmark case, the induced distance on the shape space $\mathcal{S}$ is then the shortest arc connecting the equivalence classes of the two SRVFs:

$$\rho_s([q_1], [q_2]) = \min_{(O,\gamma) \in SO(2) \times \Gamma} \arccos\left(\left\langle \left\langle q_1, O(q_2 \circ \gamma)\sqrt{\dot{\gamma}} \right\rangle \right\rangle \right). \tag{2}$$

A key point to note here is that, owing to the group structure and invariance of ρ to rotations and reparameterizations, computation of ρ_s involves optimizing only over elements of the orbit $[q_2]$ of q_2.

If the minimizers of Equation (2) are given by O^* and γ^*, we compute $q_2^* = O^*(q_2 \circ \gamma^*)\sqrt{\dot{\gamma}^*} \in [q_2]$, and construct the corresponding (geodesic) path of minimal shape deformation from q_1 to q_2^* using Equation (1) as $\alpha^*(\tau) = \frac{1}{\sin(\nu)}(\sin(\nu(1-\tau))q_1 + \sin(\nu\tau)q_2^*)$ for $\tau \in [0, 1]$, where $\nu = \rho_s([q_1], [q_2])$ as defined in Equation (2); this path allows us to efficiently visualize deformations between two shapes, and provides a qualitative meaning for the distance ρ_s.

3.3 | Registration of two shapes

An important consideration in the curve-based approach is the issue of registration or establishing correspondence between points on the observed curves. In the landmark setting, correspondence is automatically available by virtue of the labelings of the landmarks. Such a correspondence between two curves β_1 and β_2, or their SRVFs q_1 and q_2, can be established in the following manner. Since the q_i, $i = 1, 2$ share a common domain $\mathbb{S}^1$, values of q_1 and q_2 at a point $s \in \mathbb{S}^1$ can be compared. As a consequence, establishing correspondence between q_1 and q_2, or registering q_1 to q_2 (or vice versa), can be formulated as determining an element $\gamma^* \in \Gamma$ such that

$$\gamma^* := \operatorname{argmin}_{\gamma \in \Gamma} \left(\arccos(\langle\langle q_1, (q_2 \circ \gamma)\sqrt{\dot{\gamma}} \rangle\rangle) \right) = \operatorname{argmin}_{\gamma \in \Gamma} \left\| q_1 - ||q_2 \circ \gamma|| \sqrt{\dot{\gamma}} \right\|_2. \tag{3}$$

Comparing to Equation (2), we see that the optimal $\gamma^* \in \Gamma$ corresponds to the one at which the minimum preshape distance ρ is attained.

We comment briefly now on how optimization in Equation (2) is carried out. The minimizer $O^* \in SO(2)$ is computed as follows. Consider a discretization of q_i, $i = 1, 2$ obtained by sampling q_i at a fixed number of points, resulting in vectors $\boldsymbol{q}_i$, $i = 1, 2$. Let $A = \boldsymbol{q}_1 \boldsymbol{q}_2^T$, and consider its singular value decomposition (SVD) $A = USV^T$. The optimal rotation $O^* \in SO(2)$ then is $O^* = UV^T$ if the determinant of A is positive. Otherwise, one needs to modify V by changing

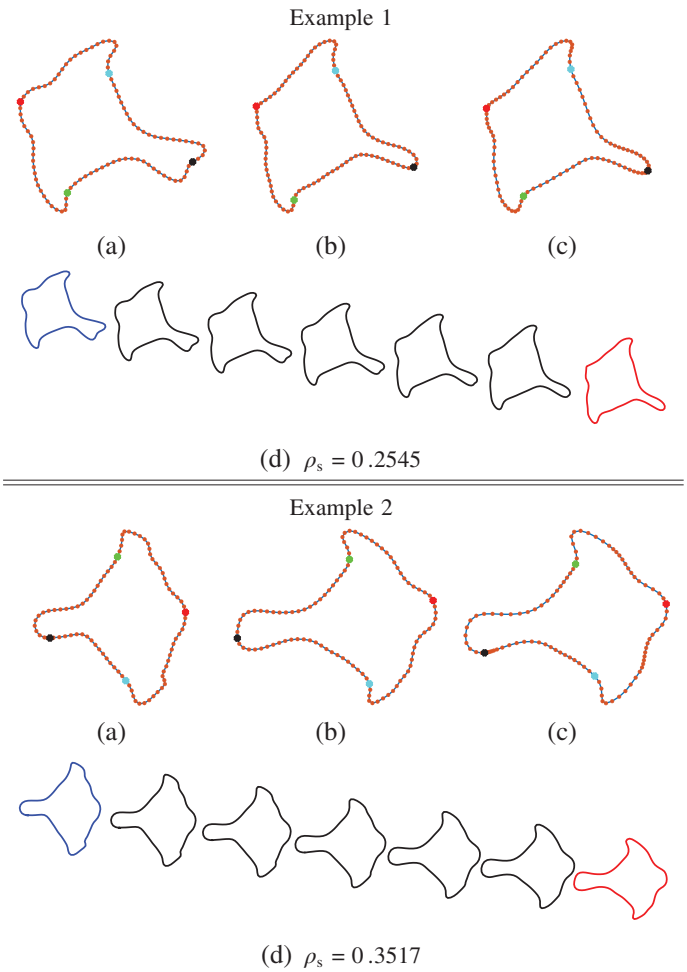

FIGURE 5 Two examples of shape distances and deformations for mouse vertebrae. (a) Shape 1. (b) Shape 2 prior to optimal reparameterization. (c) Shape 2 after optimal reparameterization. The colored points correspond to the same parameter value across the three shapes (they are not landmarks). (d) Path of minimal shape deformation and the shape distance

the sign of its last column before computing O^*. The minimizer $\gamma^* \in \Gamma$ is computed using the dynamic programming algorithm or a gradient descent approach; we omit the details of these algorithms here and refer the interested readers to Chapters 4 and 5 of Srivastava and Klassen (2016) or the PhD thesis of Robinson (2012).

Figure 5 shows two examples of pairwise comparisons of mouse vertebrae shapes. In panel (a), we display shape 1 (corresponding to the blue shape along the deformation path) sampled according to arc-length; panel (b) shows shape 2 also sampled according to arc-length. Panel (c) shows the same shape 2 optimally registered to shape 1 (corresponding to the red shape along the deformation path); note the nonlinear sampling of points along this shape. Finally, panel (d) shows the path of minimal deformation between the two shapes, discretized using seven points, and reports the corresponding shape distance (length of this path). Furthermore, Figure 6 shows the benefits of elastic shape analysis as compared to shape analysis under fixed arc-length parameterization. The elastic deformation preserves more geometric features of the shapes along the path; this is especially evident near the baseline of the "tail" portion of the vertebrae. The differences here are rather small due to shape homogeneity of the mouse vertebrae in this dataset. For more drastic examples, we refer the readers to Chapters 5 and 6 in Srivastava and Klassen (2016).

4 | STATISTICAL SUMMARIES OF SHAPES

The differences, at least operationally, between the landmark- and curve-based approaches are blurred when computing statistical summaries. This is because discretization of a curve is required for computational purposes. However, the two approaches share the complications induced by the non-Euclidean geometry of the shape space when computing a sample mean, median and principal component analysis (PCA). We shall not review the landmark-based approach separately owing to the significant overlap in the operational details.

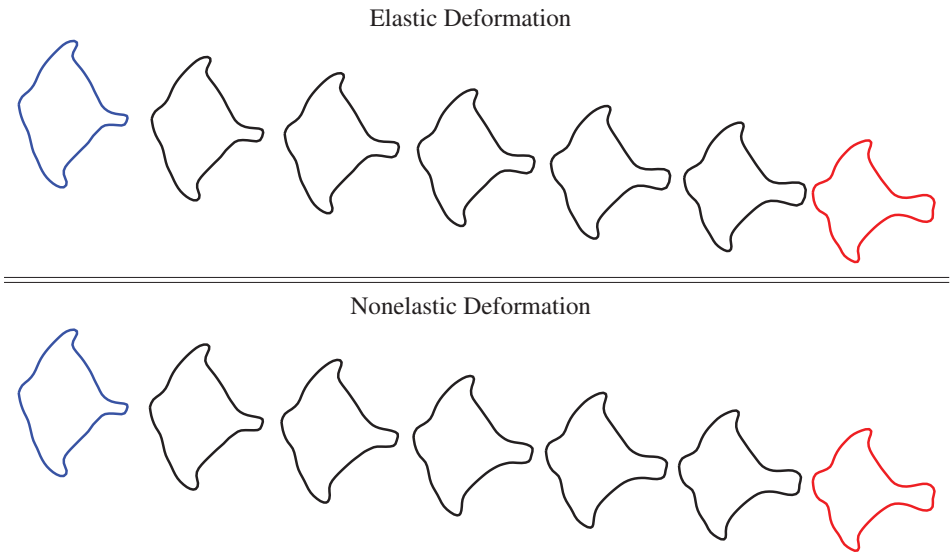

FIGURE 6 Comparison of elastic and nonelastic (based on arc-length parameterizations) shape deformations between two mouse vertebrae

Using the shape metric and the geometry of the corresponding shape space, descriptive statistical analysis is typically carried out in the following manner: (a) use the notion of a Karcher mean of a metric space, a generalization of the usual sample mean, to compute a mean shape, (b) consider a convenient linearization of the shape space around the Karcher mean shape to obtain local coordinates for the shape space, and (c) use standard multivariate techniques to carry out PCA. The approaches are mainly distinguished by the choice of the distance, and the manner in which the linearization is achieved. Intrinsic methods that avoid the linearization step have also been proposed (Fletcher, Lu, Pizer, & Joshi, 2004; Zhang & Fletcher, 2013, 2014), but will not be discussed here.

4.1 | Computing mean shape

The sample Karcher mean of a collection of points $x_1, ..., x_n$ from a metric space $(\mathfrak{X}, d)$ is defined as the minimizer of the sum of squared distances to x_i:

$$\hat{\mu} = \text{argmin}_{x \in \mathfrak{X}} \sum_{i=1}^{n} d(x, x_i)^2. \tag{4}$$

This generalizes the definition of the sample mean in Euclidean space as the minimizer of the functional $y \mapsto 1/n \sum_{i=1}^{n} |y - x_i|^2$. Evidently, the definition is applicable to the metric shape spaces for landmark-based and curve-based approaches for specific choices of $\mathfrak{X}$ and distance d. If only distances (and not their squares) are used in the definition, then the minimizer is a sample median (Fletcher, Venkatasubramanian, & Joshi, 2009). We will focus on the Karcher mean.

Elements of the shape space $\mathcal{S}$ are equivalence classes or orbits. One way to understand the orbit representing a Karcher mean shape, although not always in an equivalent sense, is as the shape of the Karcher mean. In other words, if $\hat{\mu}$ is the sample mean computed using Equation (4) on the preshape space $\mathcal{C}$ based on the shape distance ρ_s, then we can regard its orbit $[\hat{\mu}]$ as the mean shape. Furthermore, the average of squared shape distances from each sample shape to the shape mean $\hat{\mu}$ gives the so-called Karcher variance, an overall measure of spread in the sample. From this perspective, owing to the definition of the shape distance ρ_s in Equation (2), we can view computation of the mean as an optimization problem over the preshape space $\mathcal{C}$. That is, given curves $\beta_1, ..., \beta_n$, their SRVFs $q_1, ..., q_n$ are points on the preshape space $\mathcal{C}$. We can compute the Karcher mean $\hat{\mu}$ with respect to the shape distance ρ_s as the minimizer of the functional $\mathcal{C} \ni q \mapsto \sum_{i=1}^{n} \rho_s([q], [q_i])^2$. This amounts to computing

$$\hat{\mu} = \text{argmin}_{q \in \mathcal{C}} \sum_{i=1}^{n} \left[\min_{[O_i, \gamma_i] \in SO[2] \times \Gamma} \arccos(\langle \langle q, O_i [q_i \circ \gamma_i] \sqrt{\dot{\gamma}_i} \rangle \rangle) \right]^2.$$

The mean shape is then considered to be the orbit $[\hat{\mu}]$ of $\hat{\mu}$. From our earlier discussion on registration between curves, we note that computing the mean using the expression above entails registering each q_i to the eventual Karcher mean $\hat{\mu}$. This will be profitably used when carrying out PCA on the shape space.

Computation of the Karcher mean is carried out using gradient-based algorithms (Le, 2001; Pennec, 2006); a detailed algorithm for computing this shape statistic under the SRVF representation is given in Kurtek et al. (2013). Note that the final solution obtained via these algorithms may only be a local minimum. The algorithms iterate between three steps: (a) project all shapes to the tangent space at the current estimate of the mean, (b) compute the gradient of the appropriate cost function, and (c) update the current estimate of the mean on the preshape space $\mathcal{C}$. The first and third steps require geometric tools called the inverse-exponential and exponential maps (reviewed in the next subsection), which allow one to project points from a manifold to a linear tangent space and vice versa.

4.2 | PCA on shape space

Exploration of variability in a sample of shape data can be carried out by choosing a suitable set of coordinates in the vicinity of the Karcher mean $\hat{\mu}$. The Riemannian framework provides a convenient formalism to choose local coordinates. In particular, the Euclidean coordinates of the tangent space $T_{\hat{\mu}}(\mathcal{C})$ at $\hat{\mu}$ provide a convenient linearization. If the variability in the set of q_i, $i = 1, ..., n$ is not too large, then the tangent space coordinates at $\hat{\mu}$ work quite well in practice.

Using the tangent space $T_{\hat{\mu}}(\mathcal{C})$ we can access the tangent space of the mean shape $[\hat{\mu}]$ on the shape space $\mathcal{S}$. The tangent space at $\hat{\mu}$ on the preshape space can be decomposed as $T_{\hat{\mu}}(\mathcal{C}) = T_{\hat{\mu}}([\hat{\mu}]) \oplus N_{\hat{\mu}}(\mathcal{C})$, where $N_{\hat{\mu}}(\mathcal{C})$ is referred to as the perpendicular or horizontal space consisting of functions in $\mathcal{C}$ that are orthogonal to the orbit $[\hat{\mu}]$. The space $N_{\hat{\mu}}(\mathcal{C})$ can be identified with the tangent space at the Karcher mean shape $[\hat{\mu}]$ in $\mathcal{S}$, denoted as $T_{[\hat{\mu}]}(\mathcal{S})$. Abusing notation, we shall denote this as $T_{\hat{\mu}}(\mathcal{S})$.

The program for performing PCA on shapes of SRVFs $q_1, ..., q_n$ is as follows:

1. Compute Karcher mean shape $\hat{\mu}$.
2. Project q_i, $i = 1, ..., n$ onto the tangent space $T_{\hat{\mu}}(\mathcal{S})$ to obtain vectors $v_1, ..., v_n$.
3. Carry out PCA on $T_{\hat{\mu}}(\mathcal{S})$ with $v_1, ..., v_n$ and then project results back onto $\mathcal{S}$.

We notice that two projections are required: in step 2 from the representation space to the tangent space at the mean $T_{\hat{\mu}}(\mathcal{S})$ (these projections are also called lifts), and in step 3 from $T_{\hat{\mu}}(\mathcal{S})$ back onto the shape space $\mathcal{S}$. The expression in Equation (1) for the shortest path between two points, by virtue of its definition, provides the two projections in the form of the exponential map $\exp_{\hat{\mu}} : T_{\hat{\mu}}(\mathcal{S}) \to \mathcal{S}$, and its inverse $\exp_{\hat{\mu}}^{-1}$. Fortunately, these are available analytically for the preshape space $\mathcal{C}$, since it is a sphere in $\mathbb{L}^2$, through which we link it to the corresponding quantities on the space $\mathcal{S}$.

The SRVFs q_i are projected onto the linear tangent space $T_{\hat{\mu}}(\mathcal{S})$ as $v_i = \exp_{\hat{\mu}}^{-1}(q_i^*)$, $i = 1, ..., n$; here, q_i^* denotes the optimally rotated and reparameterized SRVF q_i with respect to the mean $\hat{\mu}$. Denote by $\boldsymbol{v}_i$ the discretized v_i at a finite number of points M. Let $K_{2M} := 1/(n-1) \sum_{i=1}^{n} \boldsymbol{v}_i \boldsymbol{v}_i^T$ denote the $2M \times 2M$ sample covariance matrix of the vectorized $\boldsymbol{v}_i$. The matrix K_{2M} is the discretized version of the covariance kernel $K : [0, 2\pi] \times [0, 2\pi] \to \mathbb{R}$ given by $K(\omega, \tau) = (1/(n-1)) \sum_{i=1}^{n} \langle v_i(\omega), v_i(\tau) \rangle$. Notice that we do not subtract the mean from v_i (and hence $\boldsymbol{v}_i$) since the Karcher mean has been identified with the origin of the tangent space $T_{\hat{\mu}}(\mathcal{S})$ where this covariance is computed.

Standard multivariate techniques can be used now to perform PCA in the tangent space $T_{\hat{\mu}}(\mathcal{S})$ using the spectral decomposition $K_{2M} = U \Sigma U^T$. The orthonormal matrix of eigenvectors of K_{2M}, U, contains the principal components, which we refer to as the principal directions of variability in the observed shape data; the columns of U form an orthonormal PCA basis for the (discretized) tangent space $T_{\hat{\mu}}(\mathcal{S})$. The diagonal matrix Σ contains the eigenvalues of K_{2M}, usually ordered from largest to smallest, which correspond to the PC variances.

Typically, the number of observations is smaller than the dimensionality of each tangent vector: $n < 2M$. Thus, the sample covariance matrix is singular and there are at most $n - 1$ positive eigenvalues in the matrix Σ. In other words, the sample size n controls the degree of variability in the data. The submatrix formed by the first r columns of U, U_r, spans the principal subspace of the observed shape data. One can reexpress the data using coordinates of this subspace via the principal coefficients in $\mathbb{R}^r$ computed as $c_i = U_r^T \mathbf{v}_i$, $i = 1, ..., n$[2018]. One can then use these principal coefficients for further modeling, for example, PC regression (Bharath et al., 2018).

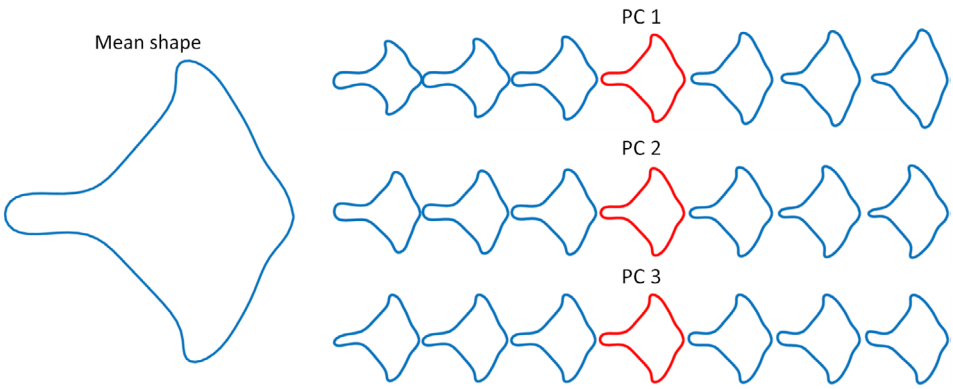

FIGURE 7 Left: Mean shape of the sample of 76 mouse vertebrae. Right: Three principal directions of shape variability, with the mean shape in red, and the three shapes to its right and left representing shapes that are one, two and three standard deviations from the mean

One can also visualize the principal directions of variation in the given shape data. This is done by following shape paths in the directions given by columns of the matrix U as follows. For a single direction given by U_j, we compute $\exp_{\hat{\mu}}\left(t\sqrt{\Sigma_{jj}}U_j\right)$, where $\exp_{\hat{\mu}}$ denotes the exponential map at $\hat{\mu}$, Σ_{jj} is the jth eigenvalue of the covariance matrix corresponding to the direction U_j, and the constant t is varied between some values $-k$ and k. Intuitively, we are following the direction U_j in the tangent space in units of standard deviation, and then projecting the results to the shape space for visualization using the exponential map.

Figure 7 displays the mean mouse vertebra shape as well as the three dominant directions of variability in the data. The patterns of deformation encoded in the PCs reflect natural variability in the "tail" and "head" portions of the vertebrae shapes.

5 | PROBABILISTIC SHAPE MODELS

There are numerous probability models for landmark shape data, usually based on distributions on the preshape space $\mathcal{C}^N$[2016] that are invariant to rotations (e.g., complex Bingham, complex Watson, complex Angular Central Gaussian; see Chapter 10 in Dryden & Mardia, 2016 for details). Such distributions assign equal mass to any rotated version of the original configuration, and hence subsequent inference is unaffected by rotational variability. Another class of models on the landmark preshape space are offset-normal models, wherein starting with a normal distribution on the configuration X, nuisance parameters such as rotations, scale and translations are integrated out with respect to uniform distributions on the parameters (see Chapter 11 of Dryden & Mardia, 2016 for details).

The infinite-dimensional nature of the preshape space $\mathcal{C}$ in the curve setting, and the infinite-dimensional nature of the space of reparameterization functions Γ, bring about some serious obstacles in defining such models: a distribution on $\mathcal{C}$ that is invariant to all possible reparameterizations does not exist; a uniform distribution on the reparameterization group Γ does not exist. Moreover, supports of probability distributions on function spaces do not generally behave like ones on finite-dimensional spaces, and exhibit some pathological properties (e.g., Gaussian distributions on $\mathbb{L}^2$ assign probability 1 or 0 to subspaces).

When sample variability is not very large, a class of models based on transforming a distribution on the tangent space of the sample Karcher mean on the preshape space, known as tangent space models, have been considered in the landmark setting (Chapter 9 in Dryden & Mardia, 2016). Extending such models to the curve setting again is complicated owing to measure-theoretic issues associated with transforming a distribution on $T_{\hat{\mu}}(\mathcal{C})$ under the exponential map $\exp_{\hat{\mu}}$[2017] (Bardelli & Mennucci, 2017).

5.1 | PCA-based and Bayesian models

A viable option in sidestepping the issues associated with the infinite-dimensionality of the shape space is to consider finite-dimensional models on the discretized curves following PCA on the shape space. Such an approach has been used in Kurtek et al. (2012) to generate random shapes in the following manner. First, estimate the Karcher mean and Karcher covariance, and perform PCA in the tangent space at the Karcher mean, in the same manner as described in

FIGURE 8 Six randomly generated mouse vertebrae shapes using a principal component analysis-based Gaussian model

the preceding section. Then, reduce dimension from $2M$ to some $k < n - 1$. Consider a k-dimensional mean zero Gaussian distribution in the tangent space, which is then wrapped onto the shape space using an appropriate mapping, for example, the exponential map or stereographic projection. Under the notation used in the preceding section, in order to generate a random sample from this model, one computes $\boldsymbol{v}_{\text{rand}} = \sum_{i=1}^{k} z_i \sqrt{\Sigma_{ii}} U_i$, where $z_i \overset{iid}{\sim} N(0,1)$. One can then rearrange the elements of $\boldsymbol{v}_{\text{rand}}$ to form a tangent vector $v_{\text{rand}} \in \mathbb{R}^{2\times M}$. We visualize the random shape associated with v_{rand} after projecting it to the shape space $\mathcal{S}$. Figure 8 displays six random mouse vertebrae shapes generated in such a manner. Note that all look structurally consistent due to the PCA-based nature of the model.

The model is easy to interpret, and generates random shapes based on dominant directions of variability in the given dataset. The z_i can follow any distribution of choice, including some heavy-tailed ones, and it hence becomes possible to generate a wide variety of random shapes, which can be viewed as suitable deformations of the sample mean shape (see also Chapter 9 of Srivastava & Klassen, 2016). Indeed, if out-of-sample prediction is of interest, then one needs to proceed with care when using this model.

Another attractive modeling option is a fully Bayesian specification using suitable prior distributions on the nuisance parameters representing rotation, scale, translation and reparameterization. Formally, consider a planar curve β with nuisance parameters (σ, O, x_0, γ) in $\mathbb{R}_+ \times SO(2) \times \mathbb{R}^2 \times \Gamma$. Let $\mathbb{P}_\mu$ be the distribution of a stochastic process $\mathbb{S}^1 \ni t \mapsto \eta(t) \in \mathbb{R}^2$ with mean function μ. Then, based on a sample of observations, $\beta_1, \ldots, \beta_n$, we can define the Bayesian model

$$\begin{aligned} &\beta_i \,|\, (\sigma_i, O_i, x_{0i}, \gamma_i, \mu) \overset{iid}{\sim} \mathbb{P}_\mu; \\ &O_i \sim \pi_1, \quad x_{0i} \sim \pi_2, \quad \sigma_i \sim \pi_3, \quad \gamma_i \sim \pi_4, \quad \mu \sim \pi_5, \end{aligned}$$

where π_1 is a distribution on $SO(2)$ (e.g., Haar measure), π_2 is any bivariate distribution on $\mathbb{R}^2$, π_3 is a distribution on the positive real line, π_4 is a distribution on the reparameterization group Γ, and π_5 is another stochastic process from $\mathbb{S}^1$ to $\mathbb{R}^2$ (e.g., Gaussian process). The set Γ is infinite-dimensional, and some suitable distributions on it have been the focus of recent work in Bharath and Kurtek (2019), Kurtek (2017), and Lu, Herbei, and Kurtek (2017). In principle, Bayesian inference on μ can be carried out using Markov chain Monte Carlo (MCMC) or other methods, although this is far from being straightforward since the dimensions of the parameters are different with some being very high. Also desirable would be to have a joint prior specification on the nuisance parameters that models the interplay between them.

5.2 | Nonparametric models

In the landmark setting, theoretical results on uniqueness of the population mean shape, consistency of the sample mean shape, and central limit theorems for the sample mean shape have been derived and studied extensively; see Bhattacharya and Bhattacharya (2012) for an excellent survey of results. Asymptotic normality of the sample mean shape can be used to develop nonparametric tests for mean shape, two-sample tests comparing populations of shapes, and other asymptotic tests. Formal asymptotic results of this nature are presently unavailable in the curve setting, and is an area of current research.

6 | RECENT ADVANCES

There have been two major recent advances that have built upon the two frameworks described in detail in this article. The first advance unifies the landmark-based and SRVF representations of shape as pictorially shown in Figure 2d. In particular, in many applications such as medicine or biology, one is interested in studying continuous shapes of objects

with additional landmark annotations. The landmark-based and elastic approaches on their own are insufficient for this purpose as they would ignore parts of the given information (either the outline or the landmarks). Strait et al. (2017) define a new landmark-constrained representation of shape, also based on the SRVF, that provides the benefits of both frameworks: curves are analyzed elastically while preserving landmark locations. Furthermore, they adapt all of the statistical tools for elastic shape analysis presented in this article to the landmark-constrained case. A similar approach to this problem is taken in Bauer, Eslitzbichler, and Grasmair (2017). However, they develop a matching functional that considers landmarks as soft constraints, that is, the landmark matching is not exact.

A closely related problem is one of automatically detecting landmarks under a formal statistical model. While in most applications the landmarks are annotated manually, this process can be tedious and expensive when the sample size is large. Strait, Chkrebtii, and Kurtek (2019) define a Bayesian statistical model to detect the number and location of landmarks on general shapes. While most work in the area of landmark detection solves this problem algorithmically, a model-based approach provides many advantages including the ability to formally assess uncertainty. The model of Strait et al. has two main components: (a) a likelihood that measures the "goodness" of the landmark set through linear shape reconstructions, and (b) prior distributions which allow the user to incorporate knowledge about the number of landmarks to select and where to place them. Inference is then performed using a reversible jump MCMC algorithm.

The SRVF representation provides a convenient setting for elastic shape analysis. However, it does not allow shape analysis under the entire family of elastic metrics; the simplicity of the SRVF framework comes at the cost of having to fix the weights for the stretching and bending terms in the elastic metric. Unfortunately, there is no guarantee that the SRVF-based weights should perform well across all applications. Rather, the choice of metric should be tied to the application of interest. Recently, there have been multiple attempts at defining computationally efficient procedures for shape analysis under the general family of elastic metrics. Bauer, Bruveris, Charon, and Moller-Andersen (2019) approximate shape distances and deformation paths under first order elastic metrics, among others, via the varifold representation. Younes (2018) generalizes the SRVF framework based on the metamorphosis viewpoint (Miller & Younes, 2001). Finally, Kurtek and Needham (2018) directly generalize the SRVF transform to accommodate the entire family of first order elastic metrics. However, much work remains to be done to define statistical procedures within these frameworks or to be able to learn optimal metric choices depending on the application and problem of interest.

7 | ADDITIONAL RESOURCES

7.1 | Available software

While this article shies away from details on computational implementation of the described landmark- and curve-based approaches to shape analysis, we point the interested readers to freely available R and Matlab software. First, many of the landmark-based shape analysis tasks can be achieved via the *shapes* package[8] in R. Similarly, shape analysis of curves, under the SRVF representation, is implemented in the *fdasrvf* package[9] in R as well as in Matlab.[10]

7.2 | Riemannian geometry books

As evident in this article, statistical shape analysis requires prerequisite knowledge in differential and Riemannian geometry. There are many excellent texts available on these topics. We suggest the books *An introduction to differentiable manifolds and Riemannian geometry* by Boothby (1975) or *Riemannian geometry* by do Carmo (1992).

7.3 | Tutorial on elastic functional and shape data analysis

Finally, we would like to direct the interested readers to materials from a recent CBMS conference on Elastic Functional and Shape Data Analysis (EFSDA),[11] which was hosted at the Mathematical Biosciences Institute in the summer of 2018. These materials contain (a) a brief, nontechnical introduction to the topic, (b) the aforementioned Matlab code for elastic shape analysis under the SRVF representation, (c) ten lectures (slides and videos) delivered primarily by Prof. Anuj Srivastava, and (d) a list of significant references.

ACKNOWLEDGMENT

The authors would like to thank Prof Ian Dryden for providing the image of the mouse vertebra used in Figure 2a.

CONFLICT OF INTEREST

The authors have declared no conflicts of interest for this article.

AUTHOR CONTRIBUTIONS

Karthik Bharath: Methodology; writing-original draft. **Sebastian Kurtek**: Methodology; writing-original draft.

ORCID

Sebastian Kurtek https://orcid.org/0000-0003-3832-9496

ENDNOTES

[1] Part of the motivation to focus on these two shape representations over others is the conceptual simplicity of the underlying mathematical frameworks in terms of requisite knowledge in Riemannian geometry.

[2] https://cran.r-project.org/web/packages/shapes/index.html

[3] Technically, the structure is not that of a product group since $OX + x_0 \neq O(X + x_0)$, and $\sigma(X + x_0) \neq (\sigma X + x_0)$, and notation should indicate a semi-direct product group $\mathbb{R}^2 \rtimes (\mathbb{R}_+ \times SO(2))$. But, we shall eschew such technicalities in this article.

[4] Technically, one should imagine this function taking values directly on the unit circle.

[5] Rather than considering orbits under the group action of scaling and translation as formulated earlier, we simply remove these sources of variability via normalization.

[6] In the case when the metric on the preshape space is invariant, it descends to the shape space, which is a quotient space of the preshape space.

[7] Technically, this preshape space is for *all* curves, open and closed; an additional closure condition is needed to restrict to closed curves only.

[8] https://cran.r-project.org/web/packages/shapes/index.html

[9] https://cran.r-project.org/web/packages/fdasrvf/index.html

[10] https://www.asc.ohio-state.edu/kurtek.1/cbms.html

[11] https://www.asc.ohio-state.edu/kurtek.1/cbms.html

RELATED WIREs ARTICLE

Statistics of shape

REFERENCES

Almhdie, A., Léger, C., Deriche, M., & Lédée, R. (2007). 3D registration using a new implementation of the ICP algorithm based on a comprehensive lookup matrix: Application to medical imaging. *Pattern Recognition Letters*, *28*(12), 1523–1533.

Bardelli, E., & Mennucci, A. C. G. (2017). Probability measures on infinite-dimensional Stiefel manifolds. *Journal of Geometric Mechanics*, *9*, 291–316.

Bauer, M., Bruveris, M., Charon, N., & Moller-Andersen, J. (2019). A relaxed approach for curve matching with elastic metrics. *ESAIM: Control, Optimisation and Calculus of Variations*, *25* (in press).

Bauer, M., Eslitzbichler, M., & Grasmair, M. (2017). Landmark-guided elastic shape analysis of human character motions. *Inverse Problems & Imaging*, *11*(4), 601–621.

Beg, M., Miller, M., Trouvé, A., & Younes, L. (2005). Computing large deformation metric mappings via geodesic flows of diffeomorphisms. *International Journal of Computer Vision*, *61*(2), 139–157.

Bharath, K., & Kurtek, S. (2019). Distribution on warp maps for alignment of closed and open curves. *Journal of the American Statistical Association*, *1708*, 04891.

Bharath, K., Kurtek, S., Rao, A., & Baladandayuthapani, V. (2018). Radiologic image-based statistical shape analysis of brain tumours. *Journal of the Royal Statistical Society, Series C*, *67*(5), 1357–1378.

Bhattacharya, A. & Bhattacharya, R. (2012). Nonparametric inference on manifolds: With applications to shape spaces. IMS monographs.

Bookstein, F. L. (1984). A statistical method for biological shape comparisons. *Journal of Theoretical Biology*, *107*(3), 475–520.

Bookstein, F. L. (1992). *Morphometric tools for landmark data: Geometry and biology*. Cambridge, MA: Cambridge University Press.

Bookstein, F. L. (1996). Biometrics, biomathematics and the morphometric synthesis. *Bulletin of Mathematical Biology*, *58*(2), 313–365.

Boothby, W. M. (1975). *An introduction to differentiable manifolds and Riemannian geometry*. In *Pure and Applied Mathematics*. Astermdam: Elsevier Science.

Bouix, S., Pruessner, J. C., Collins, D. L., & Siddiqi, K. (2001). Hippocampal shape analysis using medial surfaces. *NeuroImage*, *25*, 1077–1089.

Charon, N., & Truové, A. (2013). The varifold representation of nonoriented shapes for diffeomorphic registration. *SIAM Journal of Imaging Science*, *6*(4), 2547–2580.

Cheng, W., Dryden, I. L., & Huang, X. (2016). Bayesian registration of functions and curves. *Bayesian Analysis*, *11*(2), 447–475.

Cho, M.-H., Asiaee, A., & Kurtek, S. (2019). Elastic statistical shape analysis of biological structures with case studies: A tutorial. *Bulletin of Mathematical Biology*, *81*(7), 2052–2073.

Crawford, L., Monod, A., Chen, A. X., Mukherjee, S., & Rabadán, R. (2019). *Functional data analysis using a topological summary statistic: The smooth Euler characteristic transform*. arXiv:1611.06818v4.

do Carmo, M. P. (1992). *Riemannian geometry*. Basel: Birkhäuser.

Dryden, I. L., & Mardia, K. V. (1993). Multivariate shape analysis. *Sankhya, Series A*, *55*(3), 460–480.

Dryden, I. L., & Mardia, K. V. (2016). *Statistical shape analysis: With applications in R* (2nd ed.). New York, NY: Wiley.

Durrleman, S., Pennec, X., Trouvé, A., & Ayache, N. (2009). Statistical models of sets of curves and surfaces based on currents. *Medical Image Analysis*, *13*(5), 793–808.

Fletcher, P. T., Lu, C., Pizer, S. M., & Joshi, S. C. (2004). Principal geodesic analysis for the study of nonlinear statistics of shape. *IEEE Transactions on Medical Imaging*, *23*(8), 995–1005.

Fletcher, P. T., Venkatasubramanian, S., & Joshi, S. (2009). The geometric median on Riemannian manifolds with application to robust atlas estimation. *NeuroImage*, *45*(1), S143–S152.

Glaunès, J., Qiu, A., Miller, M. I., & Younes, L. (2008). Large deformation diffeomorphic metric curve mapping. *International Journal of Computer Vision*, *80*(3), 317–336.

Glaunès, J., Vaillant, M., & Miller, M. I. (2004). Landmark matching via large deformation diffeomorphisms on the sphere. *Journal of Mathematical Imaging and Vision*, *20*(1), 179–200.

Gorczowski, K., Styner, M., Jeong, J. Y., Marron, J. S., Piven, J., Hazlett, H. C., … Gerig, G. (2010). Multi-object analysis of volume, pose, and shape using statistical discrimination. *IEEE Transactions on Pattern Analysis and Machine Intelligence*, *32*(4), 652–666.

Grenander, U., & Miller, M. I. (1998). Computational anatomy: An emerging discipline. *Quarterly of Applied Mathematics, LVI*, *4*, 617–694.

Humeau-Heurtier, A. (2019). Texture feature extraction methods: A survey. *IEEE Access*, *7*, 8975–9000.

Jermyn, I. H., Kurtek, S., Laga, H., & Srivastava, A. (2017). *Elastic shape analysis of three-dimensional objects*. San Rafael, CA: Morgan & Claypool Publishers.

Joshi, S. C., & Miller, M. I. (2000). Landmark matching via large deformation diffeomorphisms. *IEEE Transactions on Image Processing*, *9*(8), 1357–1370.

Joshi, S. C., Miller, M. I., & Grenander, U. (1997). On the geometry and shape of brain sub-manifolds. *Pattern Recognition and Artificial Intelligence*, *11*, 1317–1343.

Joshi, S. H., Klassen, E., Srivastava, A., & Jermyn, I. H. (2007). A novel representation for Riemannian analysis of elastic curves in $\mathbb{R}^n$. In *IEEE Conference on Computer Vision and Pattern Recognition* (pp. 1–7). New York, NY: IEEE.

Joshi, S. H., & Srivastava, A. (2009). Intrinsic Bayesian active contours for extraction of object boundaries in images. *International Journal of Computer Vision*, *81*(3), 331–355.

Kaziska, D., & Srivastava, A. (2006). Cyclostationary processes on shape spaces for gait-based recognition. In *European Conference on Computer Vision* (Vol. 3952, pp. 442–453). Gratz, Austria: LNCS.

Kendall, D. G. (1984). Shape manifolds, procrustean metrics and complex projective spaces. *Bulletin of London Mathematical Society*, *16*, 81–121.

Klassen, E., & Srivastava, A. (2006). Geodesics between 3D closed curves using path-straightening. In *European Conference on Computer Vision* (pp. 95–106). Gratz, Austria: LNCS.

Klassen, E., Srivastava, A., Mio, W., & Joshi, S. H. (2004). Analysis of planar shapes using geodesic paths on shape spaces. *IEEE Transactions on Pattern Analysis and Machine Intelligence*, *26*(3), 372–383.

Kurtek, S. (2017). A geometric approach to pairwise Bayesian alignment of functional data using importance sampling. *Electronic Journal of Statistics*, *11*(1), 502–531.

Kurtek, S., Klassen, E., Ding, Z., Jacobson, S. W., Jacobson, J. L., Avison, M. J., & Srivastava, A. (2011). Parameterization-invariant shape comparisons of anatomical surfaces. *IEEE Transactions on Medical Imaging*, *30*(3), 849–858.

Kurtek, S., & Needham, T. (2018). *Simplifying transforms for general elastic metrics on the space of plane curves*. arXiv:1803.10894v1.

Kurtek, S., Srivastava, A., Klassen, E., & Ding, Z. (2012). Statistical modeling of curves using shapes and related features. *Journal of the American Statistical Association*, *107*(499), 1152–1165.

Kurtek, S., Su, J., Grimm, C., Vaughan, M., Sowell, R., & Srivastava, A. (2013). Statistical analysis of manual segmentations of structures in medical images. *Computer Vision and Image Understanding*, *117*, 1036–1050.

Laga, H., Kurtek, S., Srivastava, A., & Miklavcic, S. J. (2014). Landmark-free statistical analysis of the shape of plant leaves. *Journal of Theoretical Biology*, *363*, 41–52.

Lang, S. (2001). Fundamentals of differential geometry. In *Graduate texts in mathematics*. Berlin: Springer.

Le, H. (2001). Locating Frechet means with application to shape spaces. *Advances in Applied Probability*, *33*(2), 324–338.

Lu, Y., Herbei, R., & Kurtek, S. (2017). Bayesian registration of functions with a Gaussian process prior. *Journal of Computational and Graphical Statistics*, *26*, 894–904.

Malladi, R., Sethian, J. A., & Vemuri, B. C. (1996). A fast level set based algorithm for topology-independent shape modeling. *Journal of Mathematical Imaging and Vision*, *6*, 269–290.

Mardia, K. V., & Dryden, I. L. (1989). The statistical analysis of shape data. *Biometrika*, *76*(2), 271–281.

Materka, A. (2004). Texture analysis methodologies for magnetic resonance imaging. *Dialogues in Clinical Neuroscience*, *6*(2), 243–250.

Miller, M. I., & Younes, L. (2001). Group actions, homeomorphisms, and matching: A general framework. *International Journal of Computer Vision*, *41*(1–2), 61–84.

Mio, W., Srivastava, A., & Joshi, S. H. (2007). On shape of plane elastic curves. *International Journal of Computer Vision*, *73*(3), 307–324.

O'Higgins, P., & Dryden, I. L. (1992). Studies of craniofacial development and evolution. *Archaeology and Physical Anthropology in Oceania*, *27*, 105–112.

Pennec, X. (2006). Intrinsic statistics on Riemannian manifolds: Basic tools for geometric measurements. *Journal of Mathematical Imaging and Vision*, *25*(1), 127–154.

Robinson, D. T. (2012). *Functional data analysis and partial shape matching in the square root velocity framework* (PhD thesis). Florida State University.

Samir, C., Kurtek, S., Srivastava, A., & Canis, M. (2014). Elastic shape analysis of cylindrical surfaces for 3D/2D registration in endometrial tissue characterization. *IEEE Transactions on Medical Imaging*, *33*(5), 1035–1043.

Samir, C., Srivastava, A., Daoudi, M., & Klassen, E. (2009). An intrinsic framework for analysis of facial surfaces. *International Journal of Computer Vision*, *82*(1), 80–95.

Siddiqi, K., & Pizer, S. (2008). *Medial representations: Mathematics, algorithms and applications*. Berlin: Springer.

Small, C. G. (1996). *The statistical theory of shape*. Berlin: Springer.

Srivastava, A., Klassen, E., Joshi, S. H., & Jermyn, I. H. (2011). Shape analysis of elastic curves in Euclidean spaces. *IEEE Transactions on Pattern Analysis and Machine Intelligence*, *33*, 1415–1428.

Srivastava, A., & Klassen, E. P. (2016). *Functional and shape data analysis*. Berlin: Springer-Verlag.

Srivastava, A., Samir, C., Joshi, S. H., & Daoudi, M. (2009). Elastic shape models for face analysis using curvilinear coordinates. *Journal of Mathematical Imaging and Vision*, *33*(2), 253–265.

Strait, J., Chkrebtii, O., & Kurtek, S. (2019). Automatic detection and uncertainty quantification of landmarks on elastic curves. *Journal of the American Statistical Association*, *114*, 1002–1017. https://doi.org/10.1080/01621459.2018.1527224

Strait, J., Kurtek, S., Bartha, E., & MacEachern, S. N. (2017). Landmark-constrained elastic shape analysis of planar curves. *Journal of the American Statistical Association*, *112*(518), 521–533.

Su, J., Kurtek, S., Klassen, E., & Srivastava, A. (2014). Statistical analysis of trajectories on Riemannian manifolds: Bird migration, hurricane tracking and video surveillance. *Annals of Applied Statistics*, *8*(1), 530–552.

Thompson, D. (1917). *On growth and form*. Cambridge, MA: Cambridge University Press.

Vaillant, M., & Glaunès, J. (2005). Surface matching via currents. In *Information processing in medical imaging* (pp. 381–392). Berlin, Heidelberg: Springer Berlin Heidelberg.

Younes, L. (1998). Computable elastic distance between shapes. *SIAM Journal of Applied Mathematics*, *58*(2), 565–586.

Younes, L. (2018). *Elastic distance between curves under the metamorphosis viewpoint*. arXiv:1804.10155.

Younes, L., Michor, P. W., Shah, J., Mumford, D., & Lincei, R. (2008). A metric on shape space with explicit geodesics. *Matematica E Applicazioni*, *19*(1), 25–57.

Zahn, C. T., & Roskies, R. Z. (1972). Fourier descriptors for plane closed curves. *IEEE Transactions on Computers*, *21*(3), 269–281.

Zhang, M., & Fletcher, P. T. (2013). Probabilistic principal geodesic analysis. In *Neural information processing systems* (pp. 1178–1186).

Zhang, M., & Fletcher, P. T. (2014). Bayesian principal geodesic analysis in diffeomorphic image registration. In *Medical image computing and computer-assisted intervention* (pp. 121–128). Springer International Publishing.

How to cite this article: Bharath K, Kurtek S. Analysis of shape data: From landmarks to elastic curves. *WIREs Comput Stat*. 2020;12:e1495. https://doi.org/10.1002/wics.1495